

IMECE2007-42397

**METALLIC STRUCTURAL HEAT PIPES AS SHARP LEADING EDGES
FOR MACH 7 VEHICLES**

Craig A Steeves

Department of Materials
University of California, Santa Barbara
Santa Barbara, California 93106
Email: csteeves@engineering.ucsb.edu

Ming Y He

Department of Materials
University of California, Santa Barbara
Santa Barbara, California 93106
Email: ming@engineering.ucsb.edu

Lorenzo Valdevit

Department of Materials
University of California, Santa Barbara
Santa Barbara, California 93106
Email: lorenzo@engineering.ucsb.edu

Scott Kasen

Department of Materials Science and Engineering
University of Virginia
Charlottesville, VA 22904
Email: skasen@virginia.edu

Hossein Haj-Hariri

Department of Materials Science and Engineering
University of Virginia
Charlottesville, VA 22904
Email: hh2b@virginia.edu

Haydn N G Wadley

Department of Materials Science and Engineering
University of Virginia
Charlottesville, VA 22904
Email: haydn@virginia.edu

Anthony G Evans

Department of Materials
University of California, Santa Barbara
Santa Barbara, California 93106
Email: agevans@engineering.ucsb.edu

ABSTRACT

Sharp leading edges on hypersonic vehicles experience very large heating loads and consequent high temperatures. One strategy for accommodating these effects is to provide very high effectively thermal conductivity which allows heat to be transferred from the hot leading edge to large cool surfaces for radiation into space. Heat pipes integrated within metallic leading

edges provide this function, as well as being easy to manufacture and highly robust compared to other material choices. This paper will examine the feasibility of metallic leading edge heat pipes for hypersonic vehicles in Mach 7 flight. Using temperatures and heat fluxes calculated elsewhere, analytic approximations of the temperature distributions and stresses in a prototypical system are analyzed. The analysis is supplemented and confirmed by

finite element calculations. Feasibility of the system is assessed by simple calculations on the operational limits of heat pipes.

1 Background

For aerodynamic reasons hypersonic vehicles require sharp leading edges. Recent estimates suggest that such edges should have radius of curvature of order, $R_{le} = 3\text{mm}$. The consequent challenge is that, when the edges are that sharp, the local heat flux into the structure is intense. At the Mach numbers of interest, Mach 7 and above, the stagnation temperature, T_{st} , typically exceeds the realistic upper use temperature of most materials. Moreover, because the tip must remain sharp and have a stable shape, ablative solutions are not viable. Instead, the heat must be rapidly redistributed through the solid to enable dissipation by radiation from the largest possible area of the vehicle surface. This solution requires a concept that imparts a large effective thermal conductivity. The three primary options in this family are: (i) Carbon-based composites with anisotropic thermal conduction that retain load-bearing capability at temperatures approaching T_{st} . (ii) Ultrahigh temperature ceramics (such as HfB_2) having high melting temperatures and large thermal conductivity at $T \rightarrow T_{st}$. (iii) Heat pipes which provide exceptional thermal conductivity, enabling lower equilibrium temperatures.

This assessment addresses the role of heat pipes in metallic leading edge structures. The configuration to be addressed is a wedge-shaped vehicle with a small diameter curved leading edge surface fully-defined by the thickness t , the radius R_{le} and the angle ϕ_0 at which the curved region connects to the flat radiating surface (see figure 1). The design length of the radiating surface, L , is chosen to ensure that the materials do not exceed their maximum use temperature. The fundamental theories of heat pipe operation have been presented in such works as [1–3]. Heat pipes have been pursued in the context of leading edges and other high temperature applications [4, 5]. The present, structural, heat pipe [6] not only equilibrates the temperature but also supports transverse and shear loads (figure 2). For manufacturing facility and robustness, all-metallic designs are pursued, and their feasibility at Mach 7 deduced.

Because of the crucial role of radiation, the temperatures induced are a strong function of the emissivity, ϵ , of the radiating surface. For conventional alloys ϵ can be quite low. However, the refractory alloys to be explored can be pre-oxidized to form either alumina or silica. The most well-documented are the nickel alloys used in turbines which, when used with a bond coat, form

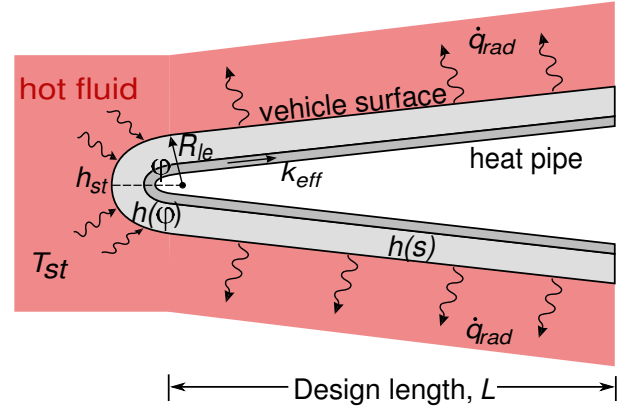


Figure 1: The local geometry and flow conditions near the leading edge.

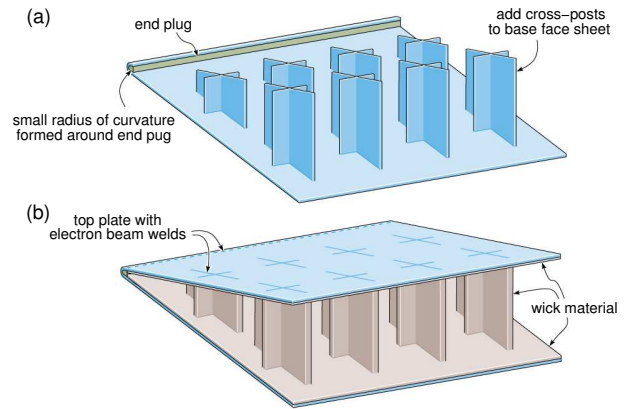


Figure 2: A structural heat pipe for the leading edge of a hypersonic vehicle. (a) A cutaway of the top surface to show the cruciform structural members. (b) The fully-assembled system with the wick material, minus the side and back surfaces.

a highly adherent, thin layer of $\alpha\text{-Al}_2\text{O}_3$. In such cases, at high temperature, $\epsilon \geq 0.9$.

The article is organized as follows: Analytic approximations for the temperatures and heat fluxes induced when the heat pipe is functioning are derived. Corresponding approximations are derived for the thermal stresses. The fidelity of these estimates of the temperatures and stresses is assessed using finite element calculations for designs based on Cb-752, a niobium alloy, which has relevant material properties: Young's modulus $E = 110\text{GPa}$, thermal expansion coefficient $\alpha = 7.4\text{ppm/K}$ and thermal conductivity $k = 48\text{W/mK}$. Other refractory alloys, such as those based on molybdenum, tungsten and rhenium, can be envisaged using the same basic protocol. The operational requirements on the heat pipe are then checked against models of heat pipe behaviour to ensure the functionality of the system in the conditions

described.

2 Analytical Estimates of Temperatures and Thermal Stresses

A method for determining the aerothermodynamic conditions at the leading edge is described elsewhere [7]. Mach 7 flight at 48 kPa dynamic pressure [8] corresponds to 29 km altitude and 2122 K stagnation temperature. The resulting stagnation point heat transfer coefficients, h_{st} are plotted in figure 3 for a range of leading edge radii.

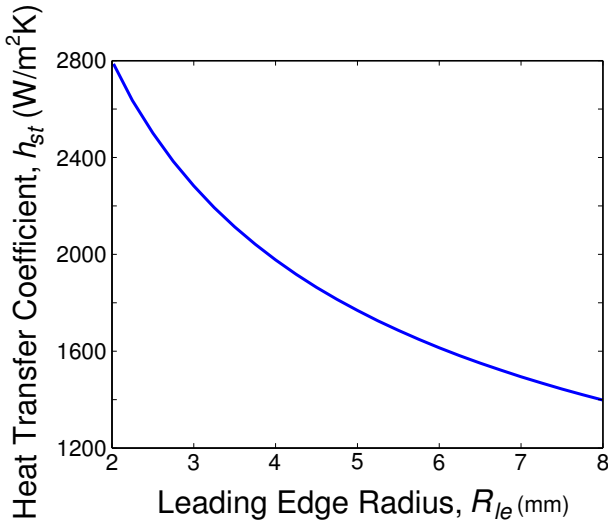


Figure 3: The stagnation point heat transfer coefficient as a function of the leading edge radius for Mach 7 flight at 29 km altitude.

Isothermal temperature. We commence with the initial assumptions that the heat pipe works perfectly and that the wall is thin, making the system effectively isothermal. This assumption will be tested later. The system is heat balanced such that all heat entering the surface through the curved leading edge is dissipated through the flat radiating surface. The heat transfer coefficient $h(\phi)$ is assumed to decline with $\cos\phi$ along the curved surface. If the isothermal system temperature is T_{iso} , the heat entering through the curved surface is given by:

$$Q_{in}^c = \int_0^{\phi_0} R_{le} h_{st} \cos\phi (T_{st} - T_{iso}) d\phi \quad (1)$$

$$\equiv R_{le} h_{st} \sin\phi_0 (T_{st} - T_{iso}).$$

Along the flat surface, if the heat transfer coefficient $h(s)$ is as-

sumed to decline with the square root of the distance from the leading edge, the convective heat transfer is given by:

$$Q_{in}^f = \int_0^L h(s) (T_{st} - T_{iso}) ds \quad (2)$$

$$\equiv 2(T_{st} - T_{iso}) h_\phi \frac{\sqrt{R}}{\tan\theta} \left(\sqrt{R + L \tan\theta} - \sqrt{R} \right).$$

with $h_\phi = h_{st} \cos(\phi_0)$ and $\theta = \pi/2 - \phi$ is the half angle of the wedge. The heat radiated out through the entire leading edge surface is:

$$Q_{out} = \int_0^{R_\phi + L} \epsilon \sigma T_{iso}^4 ds \quad (3)$$

$$\equiv \epsilon \sigma (L + R_\phi) T_{iso}^4,$$

where $\sigma = 5.67 \times 10^{-8} \text{ W/m}^2 \text{K}^4$ is the Stefan-Boltzmann constant, $R_\phi = R\phi_0$ and s is the distance along the radiating surface. Heat balance requires that $Q_{in} = Q_{out}$, and hence:

$$R_{le} h_{st} \sin\phi_0 (T_{st} - T_{iso}) + 2h_\phi \sqrt{R_\phi} (\sqrt{R_\phi + L} - \sqrt{R_\phi}) (T_{st} - T_{iso}) - \epsilon \sigma (R_\phi + L) T_{iso}^4 = 0,$$

which can be solved for T_{iso} . Results obtained for $R_{le} = 3\text{mm}$, $\phi_0 = 6^\circ$ and $\epsilon = 0.9$ are plotted in figure 4, as a function of the length of the radiating surface. The temperature T_{iso} may also be regarded as the temperature of the working fluid in the heat pipe. Note that the temperature is quite sensitive to the design length L .

Maximum temperature. The maximum temperature at the leading edge can be estimated by assessing the heat flux through the tip across a small element, length $R_{le} d\phi$ (figure 5). The curved section of the leading edge is an arc of a circle, and the temperature gradient along the stagnation line can be estimated using a one-dimensional calculation for heat flow into a hollow cylinder; this assumes that the heat flux through the wall is much larger than along the surface. The general equation for steady-state heat conduction in a hollow cylinder is:

$$k \left(\frac{\partial^2 T}{\partial r^2} + \frac{1}{r} \frac{\partial T}{\partial r} \right) = 0, \quad (5)$$

with k the thermal conductivity of the material and r the radial distance from the center. The boundary conditions are set by the

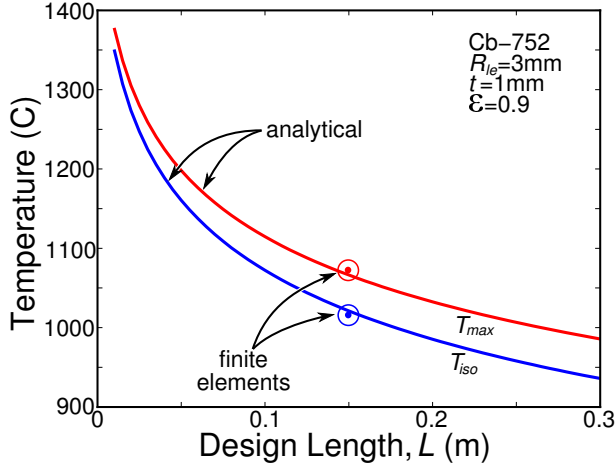


Figure 4: The leading edge temperatures for Mach 7 flight: T_{iso} , the temperature of the leading edge region under the isothermal approximation as a function of the length of the radiating surface and T_{max} , the maximum temperature at the stagnation point on the surface of the leading edge. The results for finite element calculations for the same conditions with $L = 0.15\text{m}$ are included.

stagnation temperature and heat transfer coefficient of the gas, and by the isothermal temperature on the internal surface. The maximum material temperature at the outside surface is given by:

$$T_{max} = \frac{T_{iso} + T_{st} \left(\frac{R_{le} h_{sp}}{k} \ln \frac{R_{le}}{R_i} \right)}{1 + \left(\frac{R_{le} h_{sp}}{k} \ln \frac{R_{le}}{R_i} \right)} \quad (6)$$

where $R_i = R_{le} - t$ is the inner radius of the leading edge. The solution for $R_{le} = 3\text{mm}$, $\phi = 6^\circ$ and $t = 1\text{mm}$ employing Cb-752 with $\epsilon = 0.9$ is plotted in figure 4 for various design lengths. The corresponding heat flux through the surface into the heat pipe is:

$$\dot{q} = \frac{k(T_{max} - T_{iso})}{R_i \ln \frac{R_{le}}{R_i}} \quad (7)$$

Stresses. Because the structure is metallic, yielding is of primary concern; it is assumed that buckling can be excluded through incorporation of internal lattice supports along the width (figure 2). Accordingly, the Mises stress near the leading edge where the temperature is largest, σ_{eq} , governs the integrity. Along the stagnation plane, this varies through the thickness as:

$$\sigma_{eq}(r) = \left(\frac{\sqrt{3}}{2} \right) \alpha E (T(r) - T_{iso}), \quad (8)$$

The maximum stresses induced at the exterior surface over the relevant range of Mach numbers are plotted in figure 6. Note

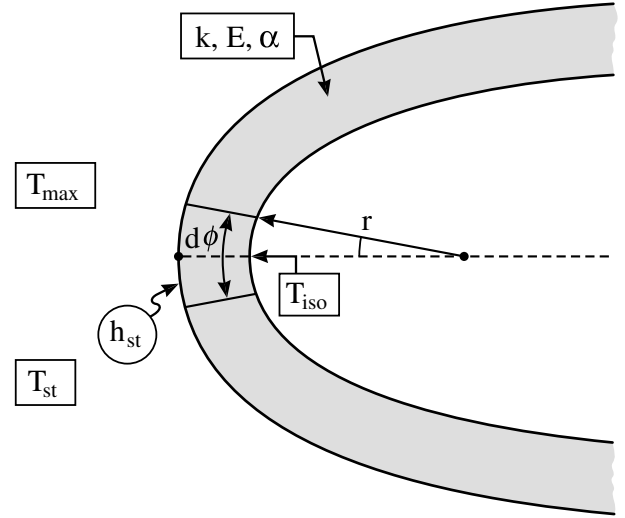


Figure 5: A sketch of the region along the stagnation line for which the temperatures are solved by an axisymmetric finite difference scheme.

that the maximum increases with larger L , despite the lower overall temperatures. This happens because, as the length increases, the total heat radiated away increases, requiring a larger thermal gradient at the leading edge to provide the larger heat flux. Importantly, the maximum stress remains below the Cb-752 yield stress at the temperatures of interest.

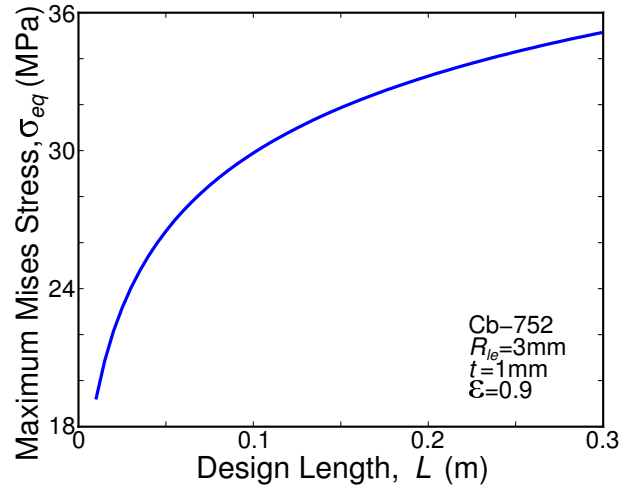


Figure 6: The maximum thermally-induced Mises stress at the exterior surface along the stagnation plane.

Failed heat pipe. In the absence of a functioning heat pipe, heat is transferred only by longitudinal conduction along the curved region into the radiating surface. Figure 7 illustrates the

behaviour of the leading edge if the heat pipe fails during Mach 7 flight. In contrast to a functioning heat pipe, the effective thermal conductivity of the leading edge is approximately two orders of magnitude smaller. Consequently, a steep temperature gradient develops along the length (figure 7) and the maximum stagnation point temperature is insensitive to the design length, remaining at approximately 1475°C for any design length. Comparison with figure 4 demonstrates the importance of having a functioning heat pipe.

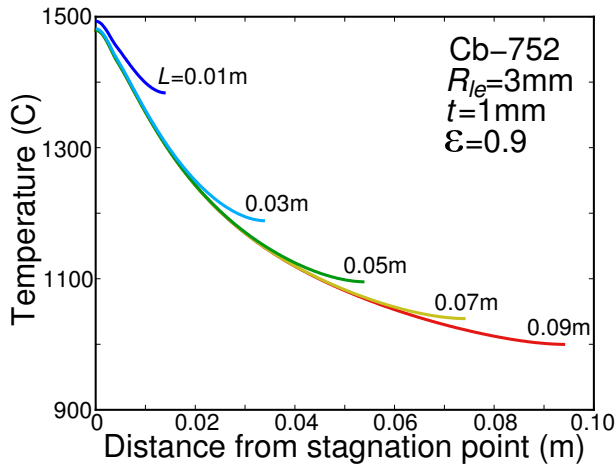


Figure 7: The behaviour of the leading edge after the heat pipe has failed: the temperature distribution along the length of the leading edge system, assuming that the material is isothermal through the thickness and that $\epsilon = 0.9$, $R_{le} = 3\text{mm}$ and $t = 1\text{mm}$.

3 Finite Element Calculations

Method. All calculations are conducted using the commercial finite element code ABAQUS. In the analysis, 8-node coupled temperature-displacement generalized plane strain elements are used. The mechanical boundary conditions are as follows (figure 8): symmetry conditions are imposed on AD in the y-direction and on CF in the x-direction.

The external thermal boundary conditions are identical to those used in the analytic model. Close to the surface, the air is assigned the stagnation temperature T_{st} , with a surface heat transfer coefficient imposed having the same spatial variation as above. Radiation to the external ambient temperature, T_{∞} is included, with emissivity $\epsilon = 0.9$. Conduction through the solid is characterized by a (temperature invariant) thermal conductivity, k . The action of the internal heat pipe is simulated by imposing

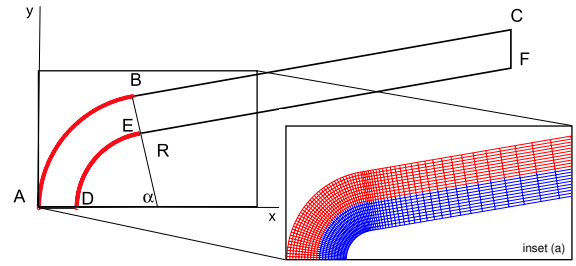


Figure 8: The domain of the finite element mesh, showing the boundary conditions, with a typical mesh near the leading edge illustrated in inset (a).

a thin (1mm) compliant layer on the inside having exceptional thermal conductivity (figure 1). This layer is assigned conductivity, $k_{hp} = 3,000\text{W/mK}$. The calculations are conducted using a niobium alloy, Cb-752, which maintains a yield strength above 200 MPa to a temperature of 1100°C.

Basic Results. The heat input and fluxes are assessed for a given design length $L = 0.15\text{m}$. Representative results are summarized in figure 9 (for emissivity $\epsilon = 0.9$). The total heat input through the external surface (figure 9(a)) increases over the curved leading segment, reaches a maximum shortly past the transition and declines thereafter due to an excess of radiation convective heat transfer. The net heat input is zero; none of the heat entering through convection remains within the vehicle: it is all dissipated by radiation. This corresponds to the isothermal condition assumed in the foregoing analytic assessment. The corresponding heat contours over the curved tip region are presented in figure 9(b). Two aspects are notable: (i) the flux entering the heat pipe near the stagnation point is large: $\dot{q}_{max} \approx 1.6\text{MW/m}^2$, though appreciably lower than the “cold wall” flux typically cited for leading edges at the same Mach number, altitude and radius; and (ii) because of the temperature uniformity enabled by the heat pipe, the radiation flux is essentially constant: $\dot{q}_{rad} \approx -140\text{kW/m}^2$.

Temperatures and Stresses. Temperatures have been obtained for the same dimensions ($R_{le} = 3\text{mm}$, $t = 1\text{mm}$, $L = 0.15\text{m}$). The interior surface attains a uniform temperature, analogous to T_{iso} in the foregoing analytic assessment. The only region that exceeds T_{iso} is the curved tip. Superimposing the analytic estimates onto the numerical results (figure 10(a)) indicates that both T_{iso} and T_{max} are very close to those predicted analyti-

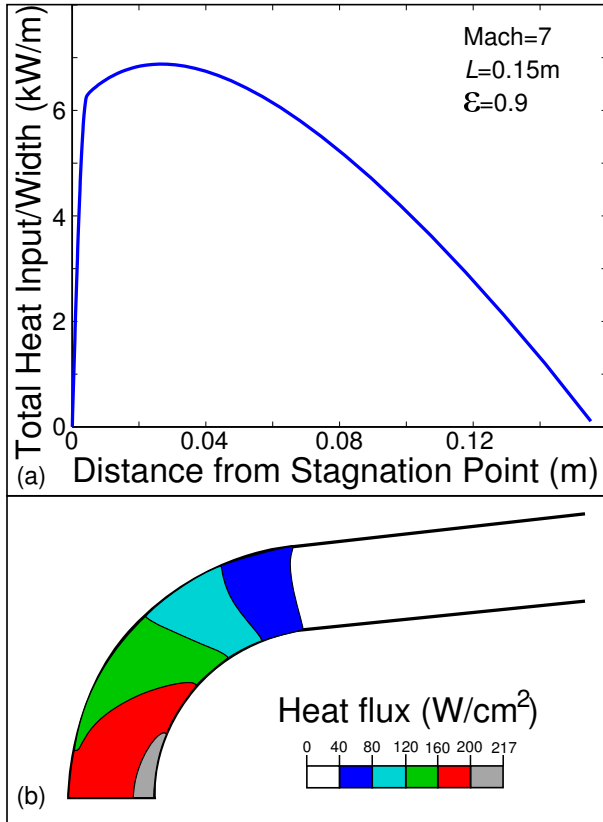


Figure 9: Heat flows at Mach 7. (a) Total heat input to the surface with distance away from the stagnation point. (b) Contours of heat flux at design length $L = 0.15\text{m}$ with $\epsilon = 0.9$.

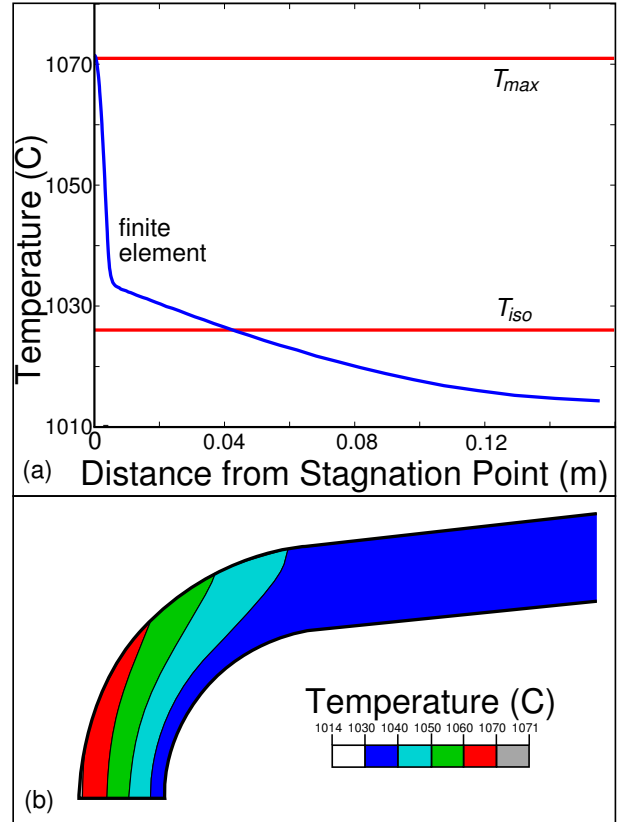


Figure 10: (a) The temperatures along the external surface as calculated by the finite element method with analytic results for T_{iso} and T_{max} in red for $\epsilon = 0.9$ superimposed. (b) Contours of the temperatures induced in the Nb-alloy at Mach 7 when the heat pipe is functioning.

cally. Contours of temperature are shown in figure 10(b). Note that T_{iso} dictates the choice of the working fluid. At Mach 7 the temperature suggests either sodium or lithium.

The Mises stresses and equivalent plastic strains have also been calculated. Contours of these stresses in the niobium alloy at Mach 7 are summarized in figure 11. Comparison with figure 6 confirms the overall accuracy of the analytical treatment above. The analytical result is lower, largely because the bending stresses are neglected. The element most susceptible to failure is that at the tip on the exterior surface where the stress and temperature are simultaneously the largest. This stress is 40 MPa, at 1071°C, below the yield strength of the material at this temperature. Consequently, the plastic strain is zero. The implication is that, provided the heat pipe is functioning, a niobium system should function at Mach 7 without failure.

4 Heat Pipe Limitations

The assumption that the heat pipe behaves as a thermal component with an effective conductivity of 3,000 W/mK over a range of operating temperatures is subject to the proviso that the isothermal temperature and the total heat flux lie within an operating envelope [2]. The boundary of the envelope is defined by a number of critical conditions. For high-temperature heat pipes, three conditions are particularly stringent: (a) the sum of the pressure losses involved in driving the operating fluid exceeds the available capillary pressure (*capillary limit*); (b) the velocity in the vapor reaches the speed of sound (*sonic limit*); and (c) the liquid in the wick boils at the wick-wall interface (*boiling limit*). Accurate estimates of these limits are necessary to ensure a robust and near-optimal design; this is beyond the scope of this work. Here we provide order-of-magnitude estimates to verify the feasibility of a niobium / niobium foam / sodium heat pipe for a Mach 7 leading edge. Details of the derivations are pro-

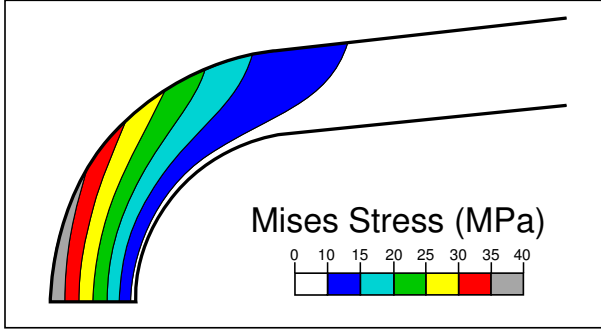


Figure 11: Mises stress and plastic strain contours when the heat pipe is functioning for Mach 7 with a niobium alloy.

vided elsewhere [1–3, 7].

Capillary limit. When the effect of gravity is neglected and total pressure recovery is assumed in the condenser, the capillary pressure needs to overcome viscous dissipation in the vapor core and in the wick, resulting in:

$$Q_{max}^{cap} = \frac{2\sigma}{r_{eff}} \left(\frac{4\mu_v L}{\rho_v h_{fg} t_v^3} + \frac{\mu_l L}{2\rho_l h_{fg} K t_w} \right)^{-1}. \quad (9)$$

Here, σ is the surface tension of the operating fluid, r_{eff} is the effective capillary radius of the wick pore, μ and ρ are the dynamic viscosity and density, h_{fg} is the latent heat of fusion, K is the permeability of the wick, and t_v and t_w are the thicknesses of the vapor and wick regions, respectively.

Sonic limit. The condition that the velocity in the vapor core is equal to the speed of sound can be expressed as:

$$Q_{max}^s = \frac{\rho_v a_v h_{fg} t_v}{\sqrt{2(\gamma+1)}}, \quad (10)$$

where $a_v = \sqrt{\gamma RT}$ is the speed of sound in the vapor, $\gamma = c_{p,v}/c_{v,v} = 1.67$, and $R = 363\text{J/kgK}$ is the gas constant for sodium vapor.

Boiling limit. The simplest expression for the heat flux that initiates boiling at the wick-wall interface can be expressed as:

$$Q_{max}^b = \frac{L_e k_{eff}}{t_w} \frac{2\sigma T_v}{h_{fg} \rho_v} \left(\frac{1}{R_b} - \frac{1}{r_{eff}} \right), \quad (11)$$

where $L_e \approx 5\text{mm}$ is the length of the evaporator, T_v the temperature of the vapor at the evaporator (assumed to be equal to the isothermal temperature), $R_b \approx 10^{-7}\text{m}$ is the average radius of the

pre-existing bubbles near the wall, and k_{eff} is the effective thermal conductivity of the permeated wick. For metal foam wicks, k_{eff} is related to the wick porosity (ψ_w) and the thermal conductivity of the solid and the liquid phase as:

$$k_{eff} = \Lambda(\psi_w k_l + (1 - \psi_w) k_s) + (1 + \Lambda) \left(\frac{\psi_w}{k_l} + \frac{1 - \psi_w}{k_s} \right)^{-1}, \quad (12)$$

where $\Lambda = 0.35$ is a fitting parameter obtained experimentally [9]. For these calculations, the wick properties and working fluid properties are taken to be those given by [2]. For sodium as the working fluid, figure 12 presents the three limits as a function of the operating temperature of the heat pipe, and defines the safe operating region (assuming $t_v = 5\text{mm}$). For a leading edge heat pipe length, $L \approx 0.15\text{m}$, the operating (isothermal) temperature is approximately 1020°C (figure 4) and the total incoming heat flux (per unit width of the vehicle) is approximately 7 kW/m (figure 9). Notice that these conditions are well within the safe envelope for a sodium heat pipe, thus verifying the initial assumption of this paper.

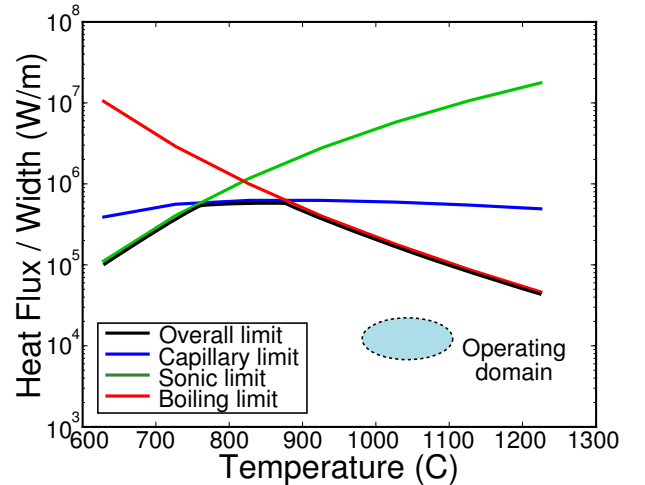


Figure 12: The three relevant operational limits and the operating envelope for a sodium heat pipe on a Mach 7 vehicle with a sharp metallic leading edge.

5 Concluding Comments

Heat pipes have been used in many contexts as a technique for spreading heat throughout a system for greater ease of dissipation. Integrated within a structural leading edge on a hypersonic vehicle, heat pipes enable material choices which are

excluded in systems without cooling, allowing easier manufacturing and more robust systems. Here the feasibility of a sodium heat pipe in a sharp (3 mm) niobium alloy leading edge on a Mach 7 vehicle has been demonstrated. By using the heat pipe to transfer the high heating localized at the stagnation point to a large radiating surface in relatively cool regions, excessive temperatures and thermal gradients can be avoided. This work can be extended to other structural materials, working fluids and vehicle velocities.

Acknowledgments

The authors would like to thank David Marshall of Teledyne, Vince Cuda of Swales Aerospace and George Jefferson of the Air Force Research Lab for discussions and very helpful assistance with this work. Funding has been provided by the Office of Naval Research through the MURI program Revolutionary Materials for Hypersonic Flight (Contract No. N00014-05-1-0439).

References

- [1] Petersen, G. P., 1994. *An Introduction to Heat Pipes: Modeling, Testing, and Applications*. John Wiley and Sons, New York.
- [2] Faghri, A., 1995. *Heat Pipe Science and Technology*. Taylor & Francis.
- [3] Reay, D. A., and Kew, P. A., 2006. *Heat Pipes: Theory, Design and Applications*, 5 ed. Butterworth Heinemann, Oxford, UK.
- [4] Glass, D. E., Camarda, C. J., Merrigan, M. A., and Sena, J. T., 1999. "Fabrication and testing of Mo-Re heat pipes embedded in carbon/carbon". *Journal of Spacecraft and Rockets*, **36**(1), January-February, pp. 79–86.
- [5] Glass, D. E., Camarda, C. J., Merrigan, M. A., Sena, J. T., and Reid, R. S., 1999. "Fabrication and testing of a leading-edge-shaped heat pipe". *Journal of Spacecraft and Rockets*, **36**(6), November, pp. 921–923.
- [6] Wadley, H. N. G., and Haj-Hariri, H., 2007. Private communication.
- [7] Steeves, C. A., Valdevit, L., He, M. Y., and Evans, A. G., 2007. "Feasibility of metallic structural heat pipes as sharp leading edges for hypersonic vehicles". In preparation, August.
- [8] Heiser, W. H., and Pratt, D., 1993. *Hypersonic Airbreathing*

Propulsion. American Institute of Aeronautics and Astronautics, Washington DC.

- [9] Carbajal, G., Sobhan, C. B., Peterson, G. P., Queheillalt, D. T., and Wadley, H. N. G., 2006. "Thermal response of a flat heat pipe sandwich structure to a localized heat flux". *International Journal of Heat and Mass Transfer*, **49**(21-22), October, pp. 4070–4081.